NANO LETTERS

pubs.acs.org/NanoLett Letter

Clustering of the Membrane Protein by Molecular Self-Assembly Downregulates the Signaling Pathway for Cancer Cell Inhibition

Ying Li, Liangbo Hu, Jing Wang, and Huaimin Wang*

Cite This: *Nano Lett.* 2024, 24, 10681−10690 Read Online

ACCESS | Metrics & More | Article Recommendations | Supporting Information

ABSTRACT: This work reports a cyclic peptide appended self-assembled scaffold that recognizes the membrane protein EGFR and arrests the EGFR signaling through multivalent interactions by assembly-induced aggregation. When incubated with cells, the oligomers of **PAD-1** first recognize the overexpressed EGFR on cancer cell membranes for arresting EGFR, which then initiates cellular uptake through endocytosis. The accumulation of **PAD-1** and EGFR in the lysosome results in the formation of nanofibers, leading to the lysosomal membrane permeabilization (LMP). These processes disrupt the homeostasis of EGFR and inhibit the downstream signaling transduction of EGFR for cancer cell survival. Moreover, LMP induced the release of protein aggregates that could generate endoplasmic reticulum (ER) stress, resulting in cancer cell death selectively. In vivo studies indicate the efficient antitumor efficiency of **PAD-1** in tumor-bearing mice. As a first example, this work provides an alternative strategy for controlling protein behavior for tuning cellular events in living cells.

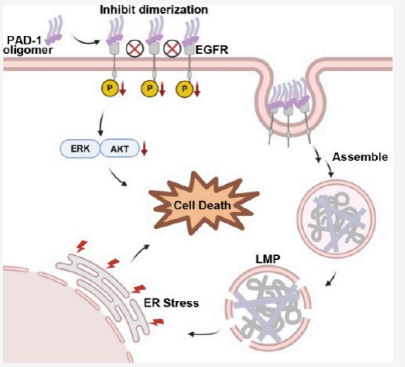

KEYWORDS: *peptide self-assembly, protein clustering and aggregation, nanofibers, cancer therapy*

Epidermal growth factor receptor (EGFR), a member of the ErbB family, is an important transmembrane receptor for signaling transduction and activation. The overexpression and abnormal activation of EGFR promote the progression of tumors.[1] Using chemical inhibitors to target EGFR for tumor inhibition has achieved a certain success. However, the acquired drug resistance and nonselectivity of their administrations limited their applications.

Protein nanoclustering plays an important role in the organization of proteins by forming mesoscale structures to form microdomains that are capable of modulating cellular signaling pathways,[2−6] including membrane receptors, transcriptional factors, and other cytosolic signaling proteins. Oligomerization of proteins enables the regulation of cellular behavior through nanoscale protein activity to microscale cellular response, thus providing general scaffolds for the assembly of protein activities in intercellular communication, proliferation, response inhibition, and immune activation. Manipulating protein clustering and aggregation in living cells is challenging because of the lack of strategies to assemble proteins at the nanoscale with tunable control and exert functions.[7] Using antibodies to cluster transmembrane receptors and chemically inducible oligomerization by small molecules are the represented techniques.[8−12] However, existing reports about artificial protein clustering/aggregation mainly focus on clustering on the cell membrane but not the intracellular region, and inhibiting tumor cell growth by clustering and aggregating EGFR is yet to be explored.

Self-assembly, as a prevalent naturally occurring process, serves as a general strategy for designing and constructing functional materials.[13−22] Recent advances in the research of peptide self-assembly in living cells stimulated research interests and efforts to explore the novel strategy to control peptide self-assembly in cells for the application of cancer therapy.[17,23−35] This work shows that the rationally designed protein aggregation driver (**PAD-1**), consisting of a self-assembly tunable motif, linkers, and EGFR ectodomain binding cyclic peptide (Figure 1A), can manipulate EGFR clustering on the cell membrane to arrest EGFR signaling transduction. Self-assembly of **PAD-1** in lysosomes can trigger EGFR to form aggregates and induce lysosomal membrane permeabilization (LMP) (Figure 1B). LMP can cause lysosomal content and protein aggregate leakage, resulting in endoplasmic reticulum (ER) stress. As a multifaceted event, the self-assembly of **PAD-1** induces necroptosis and apoptosis of cancer cells without harming normal cells. In vivo tumor-bearing mice models also indicate the anticancer efficiency of **PAD-1**.

We designed a series of **PADs** that consisted of an N-terminal capping group, a self-assembling peptide backbone, an EGFR-recognizing moiety, and a flexible linker to tune the hydrophilicity of the system. We chose the 2-naphthylacetyl

Received: July 8, 2024
Revised: August 13, 2024
Accepted: August 14, 2024
Published: August 19, 2024

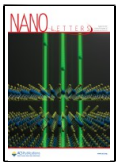

https://doi.org/10.1021/acs.nanolett.4c03217
Nano Lett. 2024, 24, 10681−10690

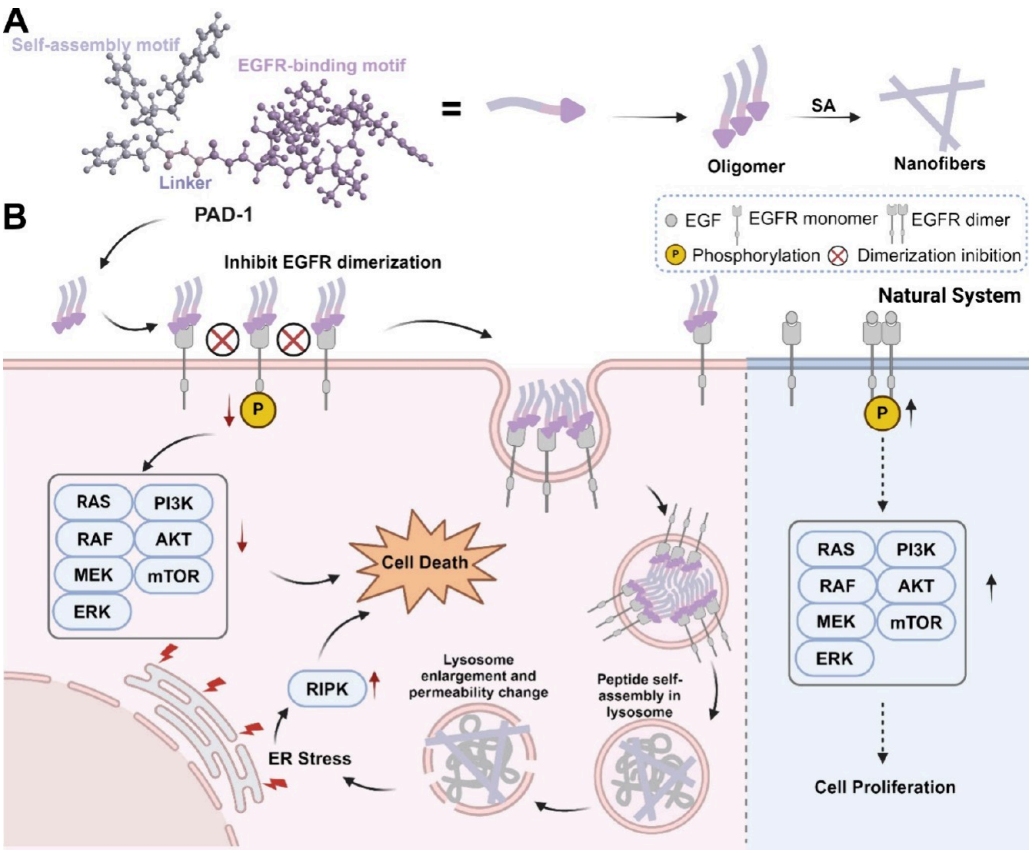

Figure 1. Schematic illustration of peptide assemblies to modulate the clustering formation of a membrane protein EGFR for cancer cell inhibition. (A) Chemical structure and the illustration of the self-assembly of **PAD-1**. (B) Illustration to show the cellular EGFR signaling pathway and the strategy for control of EGFR aggregation in this work. Peptide oligomer binds to EGFR on the cell membrane, leading to EGFR clustering on the cell membrane. After being taken up by cells through endocytosis, the oligomers self-assemble to form nanofibers with the aggregation of the protein, inducing LMP. The released protein aggregates and nanofibers cause ER stress, resulting in cancer cell death selectively. This figure was created with Biorender.com.

group to cap the N-terminal because it can provide strong intermolecular aromatic−aromatic interactions.[36] D-Phe-D-Phe (ff) is the enantiomer of a well-established peptidic backbone dipeptide Phe-Phe for self-assembly.[37] A peptide sequence **KLARLLT** (in linear or cyclic version) for binding EGFR is attached at the C-terminal of peptide.[38] Glycine (G) or poly(ethylene glycol) (PEG) usually serves as a linker to tune the system's hydrophilicity. A head-to-tail condensation reaction was used to obtain the cyclic peptide (Scheme S1). After activating the carboxyl group of **Nap-ffX** (X represents different linkers) by *N*-hydroxysuccinimide (NHS), the Nap-ffX-NHS ester reacted with the cyclic peptide via the amine group of the side chain to yield the final molecules. The identity and purity of all the molecules were confirmed by liquid chromatography−mass spectrometry (LC-MS) and ^{1}H NMR (Figures S3 to S16).

We first evaluated the cytotoxicity of **PAD**s against human cervical cancer (HeLa) cells (Figure 2B and Figure S17), which expressed high levels of EGFR.[39] Among the four linear peptides (**PAD-4** to **PAD-7**), only **PAD-4** exhibited high bioactivity against HeLa cells with an IC_{50} of 27 μM. The IC_{50} values of cyclic peptides (**PAD-1** to **PAD-3**) against HeLa cells followed the order of **PAD-3** (more than 50 μM) > **PAD-2** (25.91 μM) > **PAD-1** (0.36 μM).

The binding affinity measurements showed that the cyclic peptide had a dissociation constant (K_D) of 1.16 μM, while the linear peptide had a K_D of 1.25 μM (Table S1).[40,41] The higher binding affinity and stability of the cyclic peptide compared to the linear peptide are significant and likely contributed to the improved bioactivity of the cyclic peptide. The stability of peptides in culture medium containing 10% fetal bovine serum (FBS) was investigated and measured by LC-MS. These results (Figures S18 and S19) showed that there were two main degradation products of linear peptides, **Nap-ff-linker-K** and **Nap-ff-linker**. For **PAD-6** and **PAD-7**, the degradation ratios were close to 100% after 3 h of incubation, indicating their poor stability in culture medium. **PAD-5** also degraded by about 60%. **PAD-4** had better stability compared to the other three linear peptides, which had the lowest IC_{50} among linear peptides. These results suggested a positive correlation between their stability in the culture medium and bioactivity. For cyclic peptides, we could not observe any degraded product in LC-MS analysis even after 24 h, indicating much better stability of cyclic peptides than linear peptides (Figure S20). These results also showed that the linker between ff and the EGFR binding motif can influence the stability and final bioactivity. Moreover, the results also demonstrated that C-terminal amination (**PAD-4** and **PAD-5**) improves cancer killing efficiency, consistent with the previous report that the self-assembly ability of molecules correlates with their bioactivity.[42] Transmission electron microscopy (TEM) analysis (Figure S21) demonstrated that **PAD-1** through **PAD-4** was able to self-assemble into nanofibers. In contrast, for **PAD-5**, **PAD-6**, and **PAD-7**, only amorphous aggregates

https://doi.org/10.1021/acs.nanolett.4c03217
Nano Lett. 2024, 24, 10681−10690

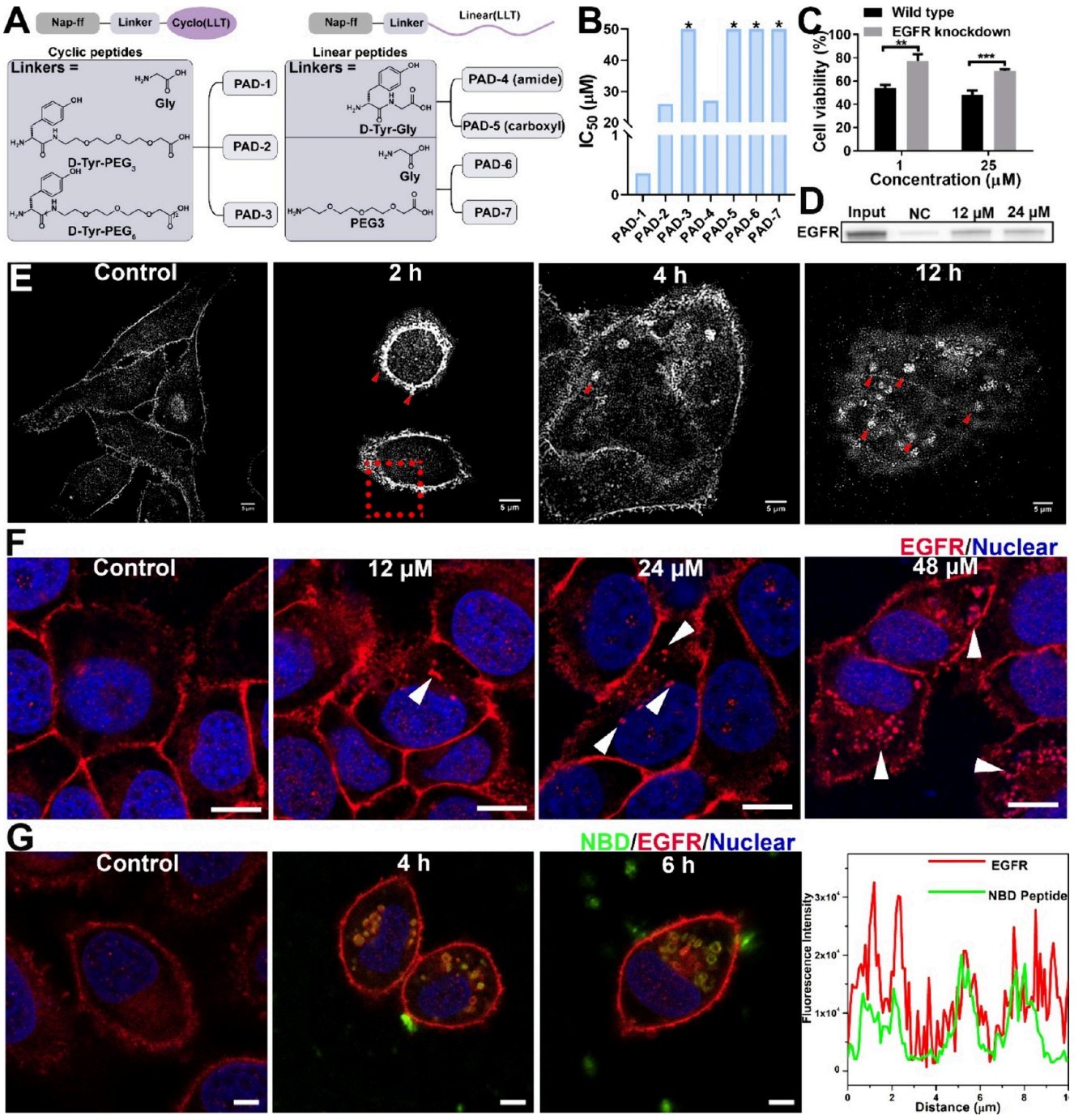

Figure 2. (A) Illustration and molecular structure of **PADs** with different linkers and EGFR binding peptide motif. (B) 48 h IC_{50} of **PADs** against HeLa cells. *, IC_{50} > 50 μM. (C) The cytotoxicity of **PAD-1** (1 and 25 μM) against wild-type HeLa cells and EGFR knockdown HeLa cells. (D) Pulldown experiment to verify the peptide−EGFR interaction; 12 and 24 μM biotin-labeled **PAD-1** co-incubates with HeLa cell lysates for 4 h in 4 °C. Clustering and aggregation of EGFR induced by **PAD-1**. (E) EGFR clusters on the cell membrane and EGFR aggregates in the cytoplasm were investigated by structured illumination microscopy. The red arrows indicate the EGFR clusters (2 h) and EGFR aggregates (4 and 12 h). (F) Immunofluorescence of HeLa cells treated with 12 μM, 24 μM, and 48 μM **PAD-1** for 24 h to show the concentration-dependent EGFR aggregates' formation. Scale bar: 10 μm. (G) The co-localization of **NBD-PAD-1** with EGFR in the lysosomes. Scale bar: 5 μm.

were observed. The circular dichroism (CD) spectra (Figure S22) of the **PADs** revealed that **PAD-1** through **PAD-4** could form a random coil-like secondary structure. However, for **PAD-5** through **PAD-7**, no distinct secondary structure was detected. The TEM and CD results suggest that the morphology and secondary structure of the **PADs** may be significant factors contributing to their bioactivity. These structural characteristics provide important insights into the potential structure−function relationships of the different **PAD** compounds.

Considering the promising bioactivity of the cyclic peptides, cytotoxicity of the cyclic peptides against different cancer cell lines was evaluated, including human osteosarcoma cells (Saos2), human hepatocellular carcinoma cells (HepG2), human non-small-cell lung cancer cells (A549), and one normal cell line, human bone marrow stromal cells (HS-5).

https://doi.org/10.1021/acs.nanolett.4c03217
Nano Lett. 2024, 24, 10681−10690

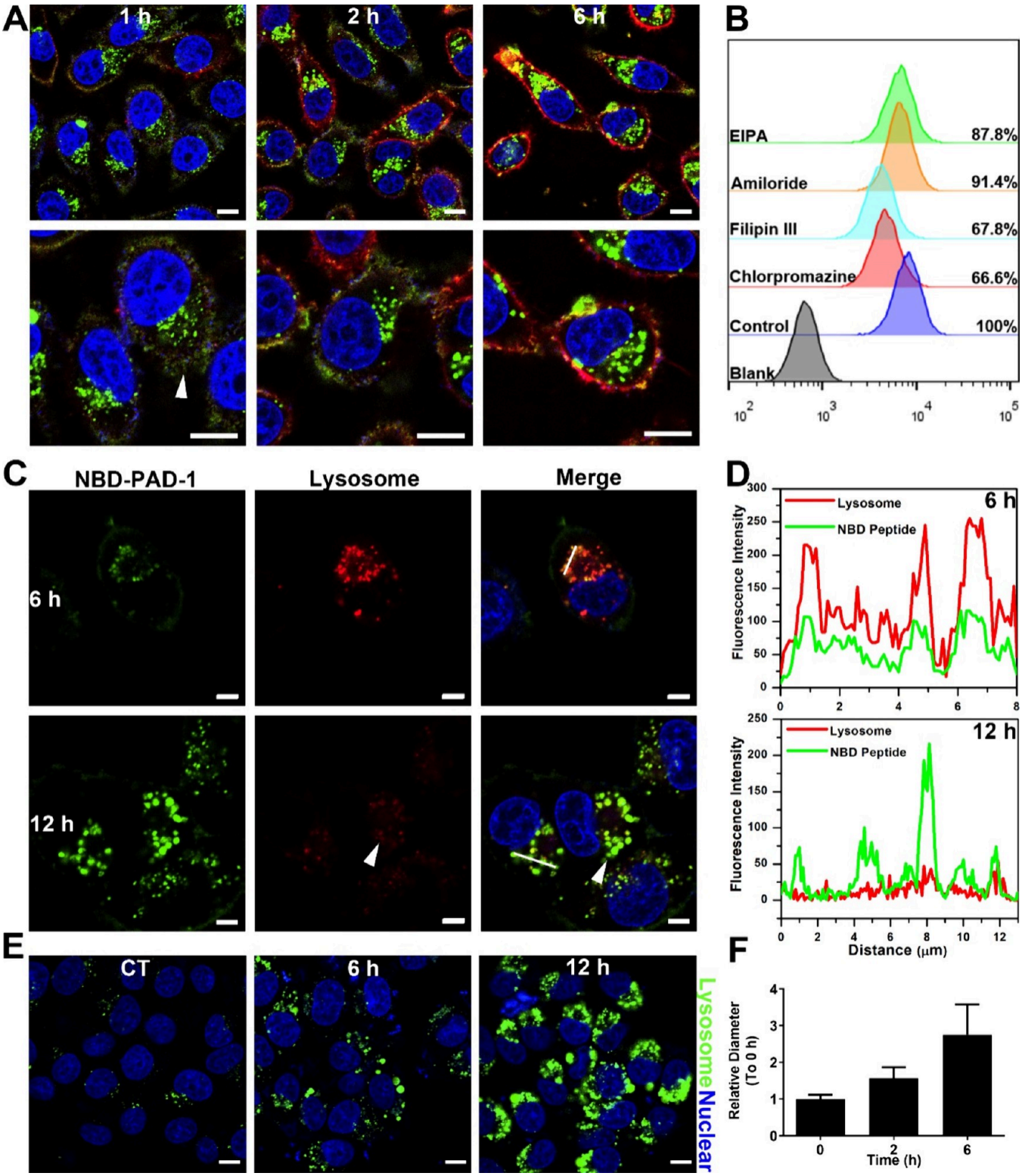

Figure 3. Cell uptake and self-assembly in living cells. (A) The cellular uptake processes of **NBD-PAD-1** (green). Cell membranes are stained by Deep Red (red). The concentration of peptide is 50 μM. Scale bar, 10 μm. (B) Effect of endocytosis inhibitors (chlorpromazine 15 μM; filipin 3 μM; amiloride 50 μM; EIPA 25 μM) on cellular uptake of 25 μM **NBD-PAD-1** for 1 h, which was analyzed by flow cytometry. (C, D) The subcellular location of **NBD-PAD-1** and the co-localization spectra of lysosome and **NBD-PAD-1**. HeLa cells were incubated with 50 μM peptide (green) for 6 and 12 h before being stained by Lyso Tracker Deep Red (red) and imaged by CLSM. Scale bar, 5 μm. (E) Cells were treated with 50 μM **PAD-1** for 6 and 12 h. Lysosome was stained by Lyso-Tracker Green. Scale bar is 5 μm. (F) The relative diameter of lysosome to control group in (E) (n = 10).

Western blotting results (Figure S23) showed that the EGFR expression level in these five cell lines follows the order of HeLa > A549 > HS-5 > HepG2 > Saos2. The IC_{50} of these three cyclic peptides against HeLa cells was much lower than

https://doi.org/10.1021/acs.nanolett.4c03217
Nano Lett. 2024, 24, 10681−10690

that against the other four cell lines (Figures S24 to S29). Among three cyclic peptides, **PAD-1** had the highest cytotoxicity against HeLa cells, the IC_{50} of which was 0.36 μM. **PAD-2** exhibits obvious cytotoxicity against normal cells (HS-5), indicating the poor selectivity of **PAD-2**. Moreover, the **NapffG** or EGFR binding motif (**Cyclo(LLT)**) was innocuous against HeLa cells (Figures S30 and S31), suggesting the importance of polyvalent properties in killing cancer cells. The critical micelle concentration (CMC) result (Figure S32) of these three cyclic peptides indicated that self-assembly ability of peptides worked with other factors inducing cytotoxicity. Based on the above results, we selected **PAD-1** for further mechanism studies.

The cytotoxicity result of **PAD-1** suggested that it may have selective activity against cells with different EGFR expression levels. To further confirm the relationship between EGFR expression and the cytotoxicity of **PAD-1**, we used small interfering RNA (siRNA) to knock down EGFR (Figure S33). The results (Figure 2C) showed that **PAD-1** exhibits less cytotoxicity against EGFR knockdown cells, indicating that the cytotoxicity of **PAD-1** positively correlates with EGFR expression in cells. Additionally, a pull-down experiment (Figure 2D) with biotin-labeled **PAD-1** further verifies that **PAD-1** can bind tightly to EGFR at the cellular level.

To study the relationship between the self-assembly ability of the peptide and the final bioactivity, we used **Ac-GGG** to replace **NapffG**, resulting in **Ac-GGG-Cyclo(LLT)** (Figures S34 and S35). The CMC of **Ac-GGG-Cyclo(LLT)** is about 288 μM, which is more than 40 times higher than the CMC of **PAD-1**. MTT experiments indicated that the **Ac-GGG-Cyclo(LLT)** has negligible cytotoxicity against HeLa cells. This suggests a positive relationship between the CMC and the final cytotoxicity of the peptides, where a higher CMC corresponds to lower cytotoxicity.

To evaluate the EGFR aggregate formation in cells after the treatment with **PAD-1**, we performed the immunofluorescent (IF) experiments to detect EGFR. The IF results obtained using structured illumination microscopy (SIM, Figure 2E) indicated that EGFR distributes uniformly on the cell membrane without any treatment. However, after 2 h of incubation with **PAD-1**, increased EGFR fluorescence intensity on the cell membrane suggested that **PAD-1** triggered the formation of EGFR clusters (Figure 2E). After 4 and 12 h of incubation, EGFR aggregates were observed in the cytoplasm, indicating that EGFR entered into cells through endocytosis to form lager aggregates. The size of artificial EGFR aggregates was obviously larger than that of natural EGFR clusters. As the incubation time increased, the amount of EGFR aggregates in the cytoplasm (red arrow) increased while the number of clusters on the cell membrane decreased. The confocal laser scanning microscopy (CLSM) result (Figure 2F) and quantification data (Figures S36 and S37) further demonstrated that the number of EGFR aggregates in the cytoplasm increased in a concentration-dependent and time-dependent manner. This suggests that the formation and accumulation of EGFR protein aggregates within the cells are directly related to both the concentration of the treatment and the duration of the exposure. The EGFR-GFP plasmid transfected HeLa cells were also utilized to investigate the formation of EGFR aggregates. The CLSM result (Figure S38) demonstrated that EGFR formed distinct protein aggregates in the cytoplasm after 6 h of incubation. To examine the location of the peptide, we replaced Nap at the N-terminus of the peptide with nitrobenzoxadiazole (NBD), resulting in **NBD-PAD-1** (Figure S39). The CLSM results (Figure 2G and Figures S40 and S41) showed that the red fluorescence from EGFR co-localized with green fluorescence from NBD. The control experiments with a single EGFR binding motif (**Cyclo(LLT)**) were also performed. The CLSM results (Figure S42) suggested that the single EGFR binding motif could not induce EGFR clustering and aggregation.

Cellular uptake processes and the distribution of molecules in the cells are significant for understanding the protein aggregate formation. The CLSM result (Figure 3A and Figure S43) showed that the green fluorescence from NBD on the cell membrane can co-localize with the red fluorescence from a cell membrane tracker (white arrows). The intensity of green fluorescence on the cell membrane decreased with an increase of time. Moreover, the green fluorescence from NBD is also located inside the cells within 1 h, which became much stronger and bigger with the increase of time, indicating that the peptide could interact with the cell membrane quickly and be taken up by the cells. By seeing the intracellular distribution of the green fluorescence and increased intensity of the green fluorescence with an increase of time, we hypothesized that the peptide could be taken up by the cells through the endocytic pathway. To investigate the possible endocytosis pathway of **PAD-1**, we used different endocytic inhibitors to co-incubate with **PAD-1**. The results (Figure 3B and Figure S44) by flow cytometry showed that the addition of amiloride (an inhibitor of macropinocytosis) and 5-(*N*-ethyl-*N*-isopropyl)amiloride (**EIPA**, another inhibitor of macropinocytosis) almost does not influence the cellular uptake of **NBD-PAD-1**. Filipin III, an inhibitor of caveolae-mediated endocytosis by disrupting the lipid raft, reduces the uptake of **NBD-PAD-1** by about 35%. Chlorpromazine (an inhibitor of clathrin-mediated endocytosis) significantly decreased the uptake of **NBD-PAD-1** by about 50%. These results indicated that **PAD-1** mainly entered cells undergoing clathrin-mediated endocytosis, and part of the peptide entered cells undergoing caveolae-mediated endocytosis.

To confirm the subcellular distribution of the peptide, lysosomes are stained with Lyso-Tracker Red. CLSM images show that the green fluorescence from NBD co-localized with the red fluorescence from Lyso-Tracker (Figure 3C,D and Figure S45) after 6 h and 12 h of co-incubation. After co-incubation for 12 h, the fluorescent intensity of NBD increased with the increase of the size of fluorescent dots. CLSM results also indicated that the intensity of red fluorescence sharply decreased after 12 and 24 h of incubation. The possible reason might be related to the disruption of lysosomes. To confirm that, another Lyso-Tracker Green was used to probe the lysosomes. The CLSM result (Figure 3E and Figure S46) showed that the edge of lysosomes (green) was clear in the control group. After 12 or 24 h of incubation of **PAD-1** with cells, diffused green fluorescence was observed in the cytoplasm, indicating that the lysosomal membrane was disrupted by the self-assembly of peptide. The measurement of the diameter of lysosomes (Figure 3F) suggested that the diameter increased after the treatment with **PAD-1** for 2 and 6 h. The diameter of lysosomes increased about 0.5 time after 2 h of incubation. From 2 to 6 h, the diameter increased about 1.5 times, indicating the enlargement of the lysosomes. These results suggest that the **PAD-1** first interacts with the cell membrane, which is then taken up by the cells through endocytosis. The accumulation of assemblies inside the

https://doi.org/10.1021/acs.nanolett.4c03217
Nano Lett. 2024, 24, 10681−10690

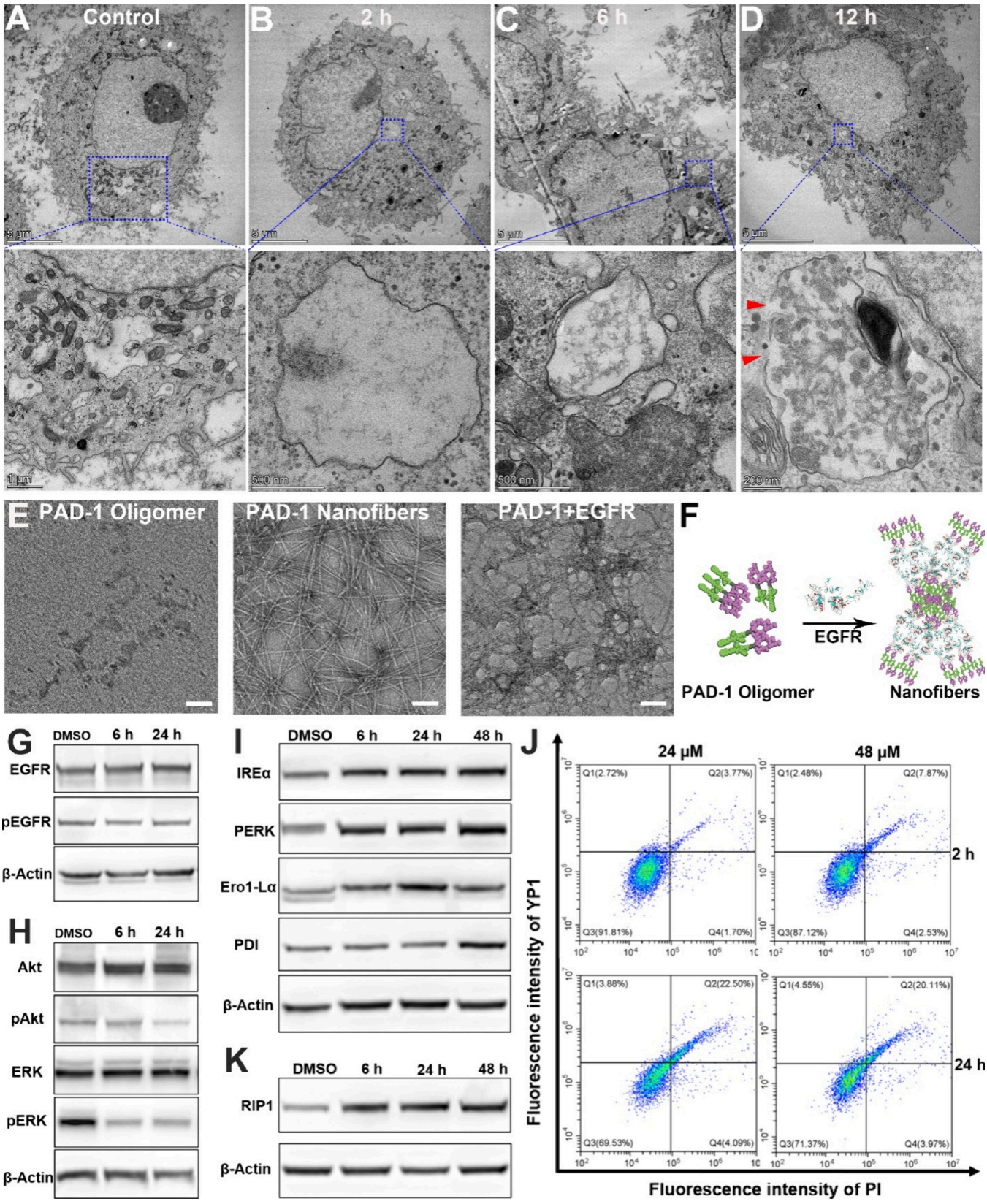

Figure 4. Bio-TEM images of HeLa cells incubated with 50 μM **PAD-1** for (A) 0, (B) 2, (C) 6, and (D) 12 h. (E) TEM images of **PAD-1** oligomer. **PAD-1** was incubated without or with EGFR in an acidic environment (pH 5.0). Scale bar: 100 nm. (F) Illustration of nanofiber formation of **PAD-1** in the presence of EGFR. Western blotting analysis of the expression level of (G) EGFR, phosphate EGFR; (H) EGFR downstream proteins: Akt, pAkt, and ERK and pERK. (I) Expression level of ER-stress markers after treatment with 50 μM **PAD-1** for different times. (J) The flow cytometry analysis of HeLa cells treated with **PAD-1** (24 or 48 μM) for 2 and 24 h by staining with PI and YP1. (K) Expression level of necroptosis-related protein after treatment with **PAD-1** (50 μM) for different times.

https://doi.org/10.1021/acs.nanolett.4c03217
Nano Lett. 2024, 24, 10681−10690

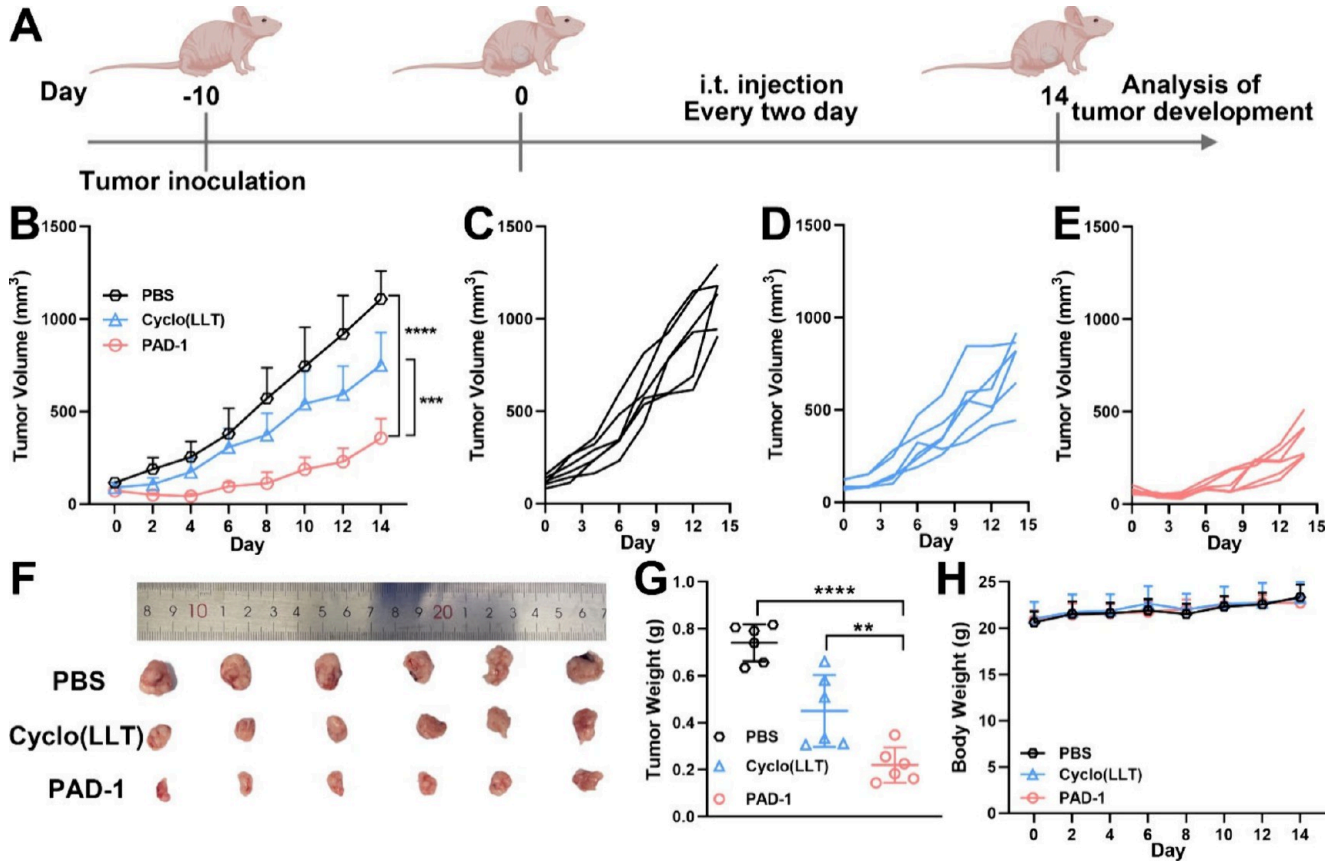

Figure 5. Antitumor efficiency in vivo. (A) Schematic illustration of treatment for subcutaneous HeLa tumor mice models with PBS, 1 mg/kg **Cyclo(LLT)**, or 1 mg/kg **PAD-1** by intratumor injection once every 2 d i.t. (intratumor). (B) The average tumor growth curves of HeLa xenografted mice after different treatments over 14 days. $n = 6$ biologically independent mice. (C−E) The individual tumor growth curves of mice in different treatment groups. (F) Photographs of dissected HeLa tumors at day 14. (G) Tumor weights in the various treatment groups on day 14. (H) Body weight changes of the various groups in the 14-day therapeutic period. Cartoon of mouse was created with Biorender.com.

lysosome could induce LMP and release the peptide assemblies and the EGFR aggregates.[43,44]

Time-dependent biological electron microscopy (Bio-EM) showed no aggregates in the lysosomes of cells without any treatment, and the lysosomal membranes maintain their integrity (Figure 4A). After 2 h of incubation of **PAD-1**, many amorphous nanostructures formed by the oligomers of peptides and EGFR (Figure 4B) can be observed in the lysosomes. With the increase of time, we can observe distinctive nanofibers and aggregates inside lysosomes (Figure 4C,D). The morphology of nanofibers observed in the Bio-EM is similar to the in vitro experiment, suggesting that the peptides self-assemble to form nanofibers in the lysosomes. Combined with the above IF results, these aggregates might be formed by the coassembly of **PAD-1** and EGFR. In addition, part of the lysosomal membrane is broken (Figure 4D, red arrow) with the increase of time, indicating that the nanofibers formed in the lysosomes can disrupt the lysosomal membrane. Except that, TEM of the **PAD-1** oligomer and assembly of **PAD-1** were also performed to verify the morphology change. The TEM result (Figure 4E) showed that the initial morphology of the **PAD-1** oligomer was amorphous aggregates, which was consistent with structure observed from the 2 h incubation Bio-EM result (Figure 4B). **PAD-1** can self-assemble to form uniform nanofibers in pH 5.0, as shown in Figure 4E. However, the co-incubation of **PAD-1** with EGFR results in the formation of bundled nanofibers, as depicted in Figure 4E. This finding suggests that EGFR can enhance the assembly of **PAD-1** and may potentially coassemble with **PAD-1** to generate these bundled nanofiber structures, as illustrated in Figure 4F. The same experiment was also performed with control peptide **Cyclo(LLT)**. As shown in the TEM result (Figure S47), no new structure formed with the control peptide. Bio-EM and TEM results together suggested that there are at least three stages to form EGFR aggregates in the lysosomes: (1) the peptide oligomers interact with the EGFR and induce EGFR clustering on the cell membrane; (2) being taken up by the cells through endocytosis, the complex of peptides and EGFR self-assembly to form nanofibers in the lysosomes via noncovalent interactions. Thanks to the polyvalent properties of nanofibers binding to EGFR, EGFR is pulled into lysosomes by assemblies to form large protein aggregates; (3) peptide assemblies in the lysosome further interact with each other to form nanofibers, enlarging the lysosomal volume, resulting in lysosomal membrane permeabilization and releasing the content to the cytoplasm.

Western blotting (Figure 4G and 4H) results indicate that EGFR aggregation significantly impacts the cellular signaling pathways. **PAD-1** downregulates the phosphate EGFR (pEGFR) expression and significantly inhibits the activation of Akt and ERK, two signaling pathways related to cell proliferation.[45] The downregulation of these signaling pathways leads to cancer cell death. To confirm whether the leaked

https://doi.org/10.1021/acs.nanolett.4c03217
Nano Lett. 2024, 24, 10681−10690

nanofibers and EGFR aggregates could influence ER stress, we examined the expression levels of the unfolded protein response (UPR) and ER stress-related proteins. WB results (Figure 4I) showed that the expression level of IREα, the marker to indicate the UPR,[46] increased significantly after the treatment with **PAD-1**. Meanwhile, the expression level of PERK also sharply increased, indicating activation of the PERK signaling pathway. Time-dependent Western blotting (WB) experiments suggest that the expression level of IREα and PERK increased gradually, indicating that the signaling pathways of ER stress have been activated after 6 h of treatment of **PAD-1**.[47] The upregulation of Ero1-Lα means that there was oxidative protein.[48] The ER chaperone protein PDI is upregulated obviously after 48 h of treatment of **PAD-1**, indicating a high level of ER stress. These results suggest that **PAD-1**, which induces EGFR aggregation, can downregulate the EGFR signaling pathways and induce UPR and ER stress.

To explore the cell death mechanism, we detected the apoptosis and necroptosis of HeLa cells by flow cytometry. Compared with the cells without any treatment (Figure 4J), the cells treated with **PAD-1** exhibit similar necrosis signaling (YP1+/PI+). However, the necrosis ratio of cells increased from 3.77% (2 h) to 22.50% (24 h) after the treatment of **PAD-1**. The co-incubation of both necrostatin-1 (necroptosis inhibitor, Nec-1) and Z-VAD-FMK (apoptosis inhibitor, VAD) (Figure S48) can partially rescue **PAD-1**-induced cell death, indicating that both necroptosis and apoptosis were involved in **PAD-1**-induced cell death. WB results (Figure 4K) showed that the expression level of RIP1, a key necroptosis-related protein, increased about 3.5 times after treatment with **PAD-1** (50 μM) for 24 h. From these results, we conclude that **PAD-1** nanofibers and protein aggregates can induce ER stress, which further activates the RIPK signaling pathway, leading to cell necroptosis. The increased RIPK1 levels observed in our Western blot analysis after **PAD-1** treatment indicate the activation of the RIPK1−RIPK3−MLKL pathway associated with necroptosis. These findings demonstrate that **PAD-1** induces cell death specifically through the apoptosis and necroptosis pathway.[49−52]

The in vivo antitumor efficacy of **PAD-1** was assessed in a HeLa subcutaneous xenograft model (Figure 5). A pronounced prevention of tumor growth was observed in the mice administrated with **PAD-1** with a mean tumor volume of 356 mm^3 compared with that treated with PBS (1107 mm^3) and **Cyclo(LLT)** (702 mm^3) 14 days postinjection (Figure 5B). **PAD-1** showed about 70% reduction in tumor volume growth compared with the mice treated with PBS, suggesting a significant inhibition in tumor growth. The mice treated with the control peptide **Cyclo(LLT)** showed a poor tumor growth inhibition at 36%. All tumor tissues from different groups were excised for photographing, weighing, and analysis (Figure 5F,G). The same results were obtained with the tumor weight (Figure 5G). No significant difference in body weight change was observed among the different treatment groups (Figure 5H). The TUNEL assay (Figure S49) was used to evaluate the antitumor efficacy of **PAD-1**. The results showed that **PAD-1** increased cell apoptosis in tumor tissues, compared to the PBS group and **Cyclo(LLT)** treatment group.

In summary, this work illustrates an efficient strategy for aggregating proteins in living cells through molecular self-assembly for cancer therapy. The results indicate that oligomers of the peptide on the cell membrane can bind to EGFR and arrest EGFR signaling. After cellular uptake through endocytosis, the coassemblies of peptide and EGFR can form large nanofibrous aggregates and induce LMP, resulting in the release of the lysosomal content and nanofibers into the cytoplasm to induce UPR and ER stress. Mechanistic studies suggest that protein clustering and aggregation downregulate the essential cellular signaling pathways for cell survival. These multifaceted events, together, induced cancer cell death selectively. This work opens up a new direction for controlling molecular self-assembly for tuning cellular events in living cells, which could be helpful for designing an immunomodulation system that is required for controlling protein clustering and aggregation.[6,53]

■ ASSOCIATED CONTENT

Supporting Information

The Supporting Information is available free of charge at https://pubs.acs.org/doi/10.1021/acs.nanolett.4c03217.

Experimental materials and instruments, experimental methods, characterizations, and supplemental Figures S1−S35; MS spectra for all compounds (PDF)

■ AUTHOR INFORMATION

Corresponding Author

Huaimin Wang − *Department of Chemistry, School of Science, Westlake University; Institute of Natural Sciences, Westlake Institute for Advanced Study, Hangzhou 310024 Zhejiang Province, China;* orcid.org/0000-0002-8796-0367; Email: wanghuaimin@westlake.edu.cn

Authors

Ying Li − *Department of Chemistry, Zhejiang University, Hangzhou 310058 Zhejiang Province, China; Department of Chemistry, School of Science, Westlake University; Institute of Natural Sciences, Westlake Institute for Advanced Study, Hangzhou 310024 Zhejiang Province, China*

Liangbo Hu − *Department of Chemistry, School of Science, Westlake University; Institute of Natural Sciences, Westlake Institute for Advanced Study, Hangzhou 310024 Zhejiang Province, China*

Jing Wang − *Department of Chemistry, School of Science, Westlake University; Institute of Natural Sciences, Westlake Institute for Advanced Study, Hangzhou 310024 Zhejiang Province, China*

Complete contact information is available at: https://pubs.acs.org/10.1021/acs.nanolett.4c03217

Author Contributions

H. M. W. conceived this work. Y. L. performed the experiments and collected data. L. B. H. and J. W. performed some cell experiments. Y. L. and H. M. W. analyzed the data and wrote the manuscript with input from the other authors. All authors read and approved the manuscript. All authors have given approval to the final version of the manuscript.

Notes

The authors declare no competing financial interest.

■ ACKNOWLEDGMENTS

This project was supported by the National Natural Science Foundation of China (82272145). This research was supported by Zhejiang Provincial Natural Science Foundation of China under Grant No. XHD23C1001. This research was supported by Instrumentation and Service Centers for

Molecular Science and for Physical Science, respectively, as well as by Biomedical Research Core Facilities at Westlake University. The TOC graphic was created with BioRender.-com.

REFERENCES

(1) Arkhipov, A.; Shan, Y.; Das, R.; Endres, N. F.; Eastwood, M. P.; Wemmer, D. E.; Kuriyan, J.; Shaw, D. E. Architecture and membrane interactions of the egf receptor. *Cell* **2013**, *152* (3), 557−569.
(2) Varma, R.; Mayor, S. Gpi-anchored proteins are organized in submicron domains at the cell surface. *Nature* **1998**, *394* (6695), 798−801.
(3) Goswami, D.; Gowrishankar, K.; Bilgrami, S.; Ghosh, S.; Raghupathy, R.; Chadda, R.; Vishwakarma, R.; Rao, M.; Mayor, S. Nanoclusters of gpi-anchored proteins are formed by cortical actin-driven activity. *Cell* **2008**, *135* (6), 1085−1097.
(4) Garcia-Parajo, M. F.; Cambi, A.; Torreno-Pina, J. A.; Thompson, N.; Jacobson, K. Nanoclustering as a dominant feature of plasma membrane organization. *J. Cell Sci.* **2014**, *127* (23), 4995−5005.
(5) Mammen, M.; Choi, S.-K.; Whitesides, G. M. Polyvalent interactions in biological systems: Implications for design and use of multivalent ligands and inhibitors. *Angew. Chem., Int. Ed.* **1998**, *37* (20), 2754−2794.
(6) Wu, H. Higher-order assemblies in a new paradigm of signal transduction. *Cell* **2013**, *153* (2), 287−292.
(7) Conway, A.; Vazin, T.; Spelke, D. P.; Rode, N. A.; Healy, K. E.; Kane, R. S.; Schaffer, D. V. Multivalent ligands control stem cell behaviour in vitro and in vivo. *Nat. Nanotechnol.* **2013**, *8* (11), 831−838.
(8) Bi, S.; Chen, W.; Fang, Y.; Wang, Y.; Zhang, Q.; Guo, H.; Ju, H.; Liu, Y. Cancer cell-selective membrane receptor clustering driven by vegf secretion for in vivo therapy. *J. Am. Chem. Soc.* **2023**, *145* (9), 5041−5052.
(9) Li, J.; Fang, Y.; Zhang, Y.; Wang, H.; Yang, Z.; Ding, D. Supramolecular self-assembly-facilitated aggregation of tumor-specific transmembrane receptors for signaling activation and converting immunologically cold to hot tumors. *Adv. Mater.* **2021**, *33* (16), No. e2008518.
(10) Li, L.; Yang, J.; Wang, J.; Kopecek, J. Amplification of cd20 cross-linking in rituximab-resistant b-lymphoma cells enhances apoptosis induction by drug-free macromolecular therapeutics. *ACS Nano* **2018**, *12* (4), 3658−3670.
(11) Cheng, D.-B.; Zhang, X.-H.; Gao, Y.-J.; Ji, L.; Hou, D.; Wang, Z.; Xu, W.; Qiao, Z.-Y.; Wang, H. Endogenous reactive oxygen species-triggered morphology transformation for enhanced cooperative interaction with mitochondria. *J. Am. Chem. Soc.* **2019**, *141* (18), 7235−7239.
(12) Wang, M. D.; Lv, G. T.; An, H. W.; Zhang, N. Y.; Wang, H. In situ self-assembly of bispecific peptide for cancer immunotherapy. *Angew. Chem., Int. Ed.* **2022**, *61* (10), 1−7.
(13) Whitesides, G. M.; Grzybowski, B. Self-assembly at all scales. *Science* **2002**, *295* (5564), 2418−2421.
(14) Aida, T.; Meijer, E.; Stupp, S. Functional supramolecular polymers. *Science* **2012**, *335* (6070), 813−817.
(15) Feng, Z.; Zhang, T.; Wang, H.; Xu, B. Supramolecular catalysis and dynamic assemblies for medicine. *Chem. Soc. Rev.* **2017**, *46* (21), 6470−6479.
(16) Rudra, J. S.; Tian, Y. F.; Jung, J. P.; Collier, J. H. A self-assembling peptide acting as an immune adjuvant. *Proc. Natl. Acad. Sci. U. S. A.* **2010**, *107* (2), 622−627.
(17) Ding, Y.; Zheng, D.; Xie, L.; Zhang, X.; Zhang, Z.; Wang, L.; Hu, Z.-W.; Yang, Z. Enzyme-instructed peptide assembly favored by preorganization for cancer cell membrane engineering. *J. Am. Chem. Soc.* **2023**, *145* (8), 4366−4371.
(18) Liang, G.; Ren, H.; Rao, J. A biocompatible condensation reaction for controlled assembly of nanostructures in living cells. *Nat. Chem.* **2010**, *2* (1), 54−60.
(19) Smith, D. J.; Brat, G. A.; Medina, S. H.; Tong, D.; Huang, Y.; Grahammer, J.; Furtmüller, G. J.; Oh, B. C.; Nagy-Smith, K. J.; Walczak, P.; et al. A multiphase transitioning peptide hydrogel for suturing ultrasmall vessels. *Nat. Nanotechnol.* **2016**, *11* (1), 95−102.
(20) Su, H.; Wang, F.; Ran, W.; Zhang, W.; Dai, W.; Wang, H.; Anderson, C. F.; Wang, Z.; Zheng, C.; Zhang, P.; et al. The role of critical micellization concentration in efficacy and toxicity of supramolecular polymers. *Proc. Natl. Acad. Sci. U. S. A.* **2020**, *117* (9), 4518−4526.
(21) Lock, L. L.; Reyes, C. D.; Zhang, P.; Cui, H. Tuning cellular uptake of molecular probes by rational design of their assembly into supramolecular nanoprobes. *J. Am. Chem. Soc.* **2016**, *138* (10), 3533−3540.
(22) Lin, Y. C.; Lim, Y. F.; Russo, E.; Schneider, P.; Bolliger, L.; Edenharter, A.; Altmann, K. H.; Halin, C.; Hiss, J. A.; Schneider, G. Multidimensional design of anticancer peptides. *Angew. Chem., Int. Ed.* **2015**, *54* (35), 10370−10374.
(23) Chagri, S.; Ng, D. Y.; Weil, T. Designing bioresponsive nanomaterials for intracellular self-assembly. *Nat. Rev. Chem.* **2022**, *6* (5), 320−338.
(24) Wang, H.; Feng, Z.; Qin, Y.; Wang, J.; Xu, B. Nucleopeptide assemblies selectively sequester atp in cancer cells to increase the efficacy of doxorubicin. *Angew. Chem., Int. Ed.* **2018**, *57* (18), 4931−4935.
(25) Kalafatovic, D.; Nobis, M.; Son, J.; Anderson, K. I.; Ulijn, R. V. Mmp-9 triggered self-assembly of doxorubicin nanofiber depots halts tumor growth. *Biomaterials* **2016**, *98*, 192−202.
(26) Zhu, L.; Wang, T.; Perche, F.; Taigind, A.; Torchilin, V. P. Enhanced anticancer activity of nanopreparation containing an mmp2-sensitive peg-drug conjugate and cell-penetrating moiety. *Proc. Natl. Acad. Sci. U. S. A.* **2013**, *110* (42), 17047−17052.
(27) Tanaka, A.; Fukuoka, Y.; Morimoto, Y.; Honjo, T.; Koda, D.; Goto, M.; Maruyama, T. Cancer cell death induced by the intracellular self-assembly of an enzyme-responsive supramolecular gelator. *J. Am. Chem. Soc.* **2015**, *137* (2), 770−775.
(28) Zheng, Z.; Chen, P.; Xie, M.; Wu, C.; Luo, Y.; Wang, W.; Jiang, J.; Liang, G. Cell environment-differentiated self-assembly of nanofibers. *J. Am. Chem. Soc.* **2016**, *138* (35), 11128−11131.
(29) Webber, M. J.; Tongers, J.; Newcomb, C. J.; Marquardt, K.-T.; Bauersachs, J.; Losordo, D. W.; Stupp, S. I. Supramolecular nanostructures that mimic vegf as a strategy for ischemic tissue repair. *Proc. Natl. Acad. Sci. U. S. A.* **2011**, *108* (33), 13438−13443.
(30) Zheng, R.; Yang, J.; Mamuti, M.; Hou, D. Y.; An, H. W.; Zhao, Y.; Wang, H. Controllable self-assembly of peptide-cyanine conjugates in vivo as fine-tunable theranostics. *Angew. Chem., Int. Ed.* **2021**, *60* (14), 7809−7819.
(31) Yang, X.; Lu, H.; Tao, Y.; Zhou, L.; Wang, H. Spatiotemporal control over chemical assembly in living cells by integration of acid-catalyzed hydrolysis and enzymatic reactions. *Angew. Chem., Int. Ed.* **2021**, *133* (44), 23990−23997.
(32) An, H.-W.; Li, L.-L.; Wang, Y.; Wang, Z.; Hou, D.; Lin, Y.-X.; Qiao, S.-L.; Wang, M.-D.; Yang, C.; Cong, Y.; et al. A tumour-selective cascade activatable self-detained system for drug delivery and cancer imaging. *Nat. Commun.* **2019**, *10* (1), 4861. 1−15.
(33) Ren, C.; Zhang, J.; Chen, M.; Yang, Z. Self-assembling small molecules for the detection of important analytes. *Chem. Soc. Rev.* **2014**, *43* (21), 7257−7266.
(34) Yang, X.; Wu, B.; Zhou, J.; Lu, H.; Zhang, H.; Huang, F.; Wang, H. Controlling intracellular enzymatic self-assembly of peptide by host−guest complexation for programming cancer cell death. *Nano Lett.* **2022**, *22* (18), 7588−7596.
(35) Jana, B.; Jin, S.; Go, E. M.; Cho, Y.; Kim, D.; Kim, S.; Kwak, S. K.; Ryu, J.-H. Intra-lysosomal peptide assembly for the high selectivity index against cancer. *J. Am. Chem. Soc.* **2023**, *145* (33), 18414−18431.
(36) Ma, M.; Kuang, Y.; Gao, Y.; Zhang, Y.; Gao, P.; Xu, B. Aromatic− aromatic interactions induce the self-assembly of pentapeptidic derivatives in water to form nanofibers and supramolecular hydrogels. *J. Am. Chem. Soc.* **2010**, *132* (8), 2719−2728.

https://doi.org/10.1021/acs.nanolett.4c03217
Nano Lett. 2024, 24, 10681−10690

(37) Reches, M.; Gazit, E. Casting metal nanowires within discrete self-assembled peptide nanotubes. *Science* **2003**, *300* (5619), 625−627.
(38) Qamar, S.; Wang, G.; Randle, S. J.; Ruggeri, F. S.; Varela, J. A.; Lin, J. Q.; Phillips, E. C.; Miyashita, A.; Williams, D.; Ströhl, F.; et al. Fus phase separation is modulated by a molecular chaperone and methylation of arginine cation-π interactions. *Cell* **2018**, *173* (3), 720−734. e15.
(39) Capuani, F.; Conte, A.; Argenzio, E.; Marchetti, L.; Priami, C.; Polo, S.; Di Fiore, P. P.; Sigismund, S.; Ciliberto, A. Quantitative analysis reveals how egfr activation and downregulation are coupled in normal but not in cancer cells. *Nat. Commun.* **2015**, *6* (1), 1−14.
(40) Ongarora, B. G.; Fontenot, K. R.; Hu, X.; Sehgal, I.; Satyanarayana-Jois, S. D.; Vicente, M. G. H. Phthalocyanine−peptide conjugates for epidermal growth factor receptor targeting. *J. Med. Chem.* **2012**, *55* (8), 3725−3738.
(41) Williams, T. M.; Sable, R.; Singh, S.; Vicente, M. G. H.; Jois, S. D. Peptide ligands for targeting the extracellular domain of egfr: Comparison between linear and cyclic peptides. *Chemical Biology & Drug Design* **2018**, *91* (2), 605−619.
(42) Feng, Z.; Wang, H.; Chen, X.; Xu, B. Self-assembling ability determines the activity of enzyme-instructed self-assembly for inhibiting cancer cells. *J. Am. Chem. Soc.* **2017**, *139* (43), 15377−15384.
(43) Wang, J.; Hu, L.; Zhang, H.; Fang, Y.; Wang, T.; Wang, H. Intracellular condensates of oligopeptide for targeting lysosome and addressing multiple drug resistance of cancer. *Adv. Mater.* **2022**, *34* (1), No. 2104704.
(44) Jana, B.; Jin, S.; Go, E. M.; Cho, Y.; Kim, D.; Kim, S.; Kwak, S. K.; Ryu, J.-H. Intra-lysosomal peptide assembly for the high selectivity index against cancer. *J. Am. Chem. Soc.* **2023**, *145*, 18414−1843.
(45) Uribe, M. L.; Marrocco, I.; Yarden, Y. Egfr in cancer: Signaling mechanisms, drugs, and acquired resistance. *Cancers* **2021**, *13* (2748), 1−21.
(46) Cox, J. S.; Shamu, C. E.; Walter, P. Transcriptional induction of genes encoding endoplasmic reticulum resident proteins requires a transmembrane protein kinase. *Cell* **1993**, *73*, 1197−1206. June 16.
(47) Harding, H. P.; Zhang, Y.; Ron, D. Protein translation and folding are coupled by an endoplasmic-reticulum-resident kinase. *Nature* **1999**, *397* (6716), 271−274.
(48) Cabibbo, A.; Pagani, M.; Fabbri, M.; Rocchi, M.; Farmery, M. R.; Bulleid, N. J.; Sitia, R. Ero1-l, a human protein that favors disulfide bond formation in the endoplasmic reticulum. *J. Biol. Chem.* **2000**, *275* (7), 4827−4833.
(49) Wang, M.; Kaufman, R. J. The impact of the endoplasmic reticulum protein-folding environment on cancer development. *Nat. Rev. Cancer* **2014**, *14* (9), 581−597.
(50) Iurlaro, R.; Muñoz-Pinedo, C. Cell death induced by endoplasmic reticulum stress. *FEBS Journal* **2016**, *283* (14), 2640−2652.
(51) Lv, Y.; Shao, G.; Zhang, Q.; Wang, X.; Meng, Y.; Wang, L.; Huang, F.; Yang, T.; Jin, Y.; Fu, C. The antimicrobial peptide pfr induces necroptosis mediated by er stress and elevated cytoplasmic calcium and mitochondrial ros levels: Cooperation with ara-c to act against acute myeloid leukemia. *Signal Transduction and Targeted Therapy* **2019**, *4* (38), 1−3.
(52) Saveljeva, S.; Mc Laughlin, S. L.; Vandenabeele, P.; Samali, A.; Bertrand, M. J. M. Endoplasmic reticulum stress induces ligand-independent tnfr1-mediated necroptosis in l929 cells. *Cell Death & Disease* **2015**, *6* (1), e1587−e1587.
(53) Hudalla, G. A.; Sun, T.; Gasiorowski, J. Z.; Han, H.; Tian, Y. F.; Chong, A. S.; Collier, J. H. Gradated assembly of multiple proteins into supramolecular nanomaterials. *Nat. Mater.* **2014**, *13* (8), 829−836.

https://doi.org/10.1021/acs.nanolett.4c03217
Nano Lett. 2024, 24, 10681−10690